Supplementary Information for

Unveiling Synergy of Strain and Ligand Effects in Metallic Aerogel for Electrocatalytic Polyethylene Terephthalate Upcycling

Junliang Chen[a], Fangzhou Zhang[a], Min Kuang[a], Li Wang[a], Huaping Wang[a], Wei Li[b,1] and Jianping Yang[a,1]

[a]State Key Laboratory for Modification of Chemical Fibers and Polymer Materials, College of Materials Science and Engineering, Donghua University, Shanghai 201620, China

[b]Department of Chemistry, Shanghai Key Laboratory of Molecular Catalysis and Innovative Materials and State Key Laboratory of Molecular Engineering of Polymers, Fudan University, Shanghai 200433, China

[1]E-mail for corresponding author: weilichem@fudan.edu.cn; jianpingyang@dhu.edu.cn

Supplementary Figures

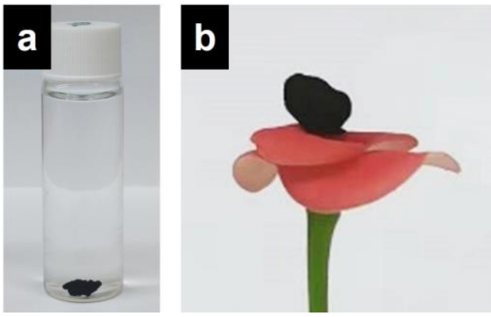

Supplementary Figure 1 Photograph images of $Pd_{67}Ag_{33}$ precursor (a) and $Pd_{67}Ag_{33}$ aerogel (b).

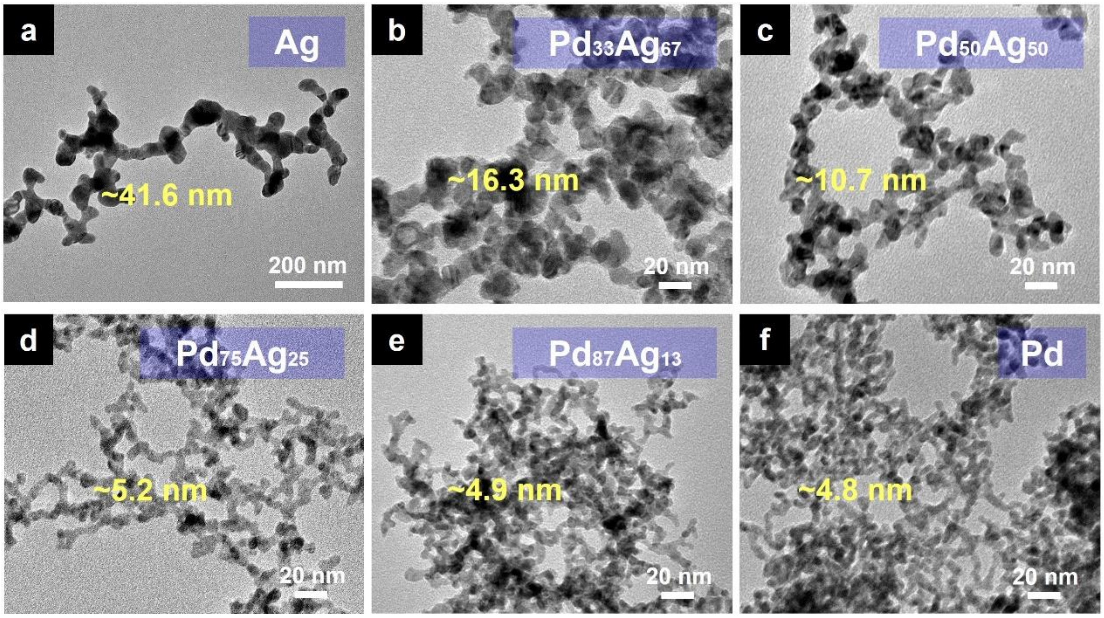

Supplementary Figure 2 TEM images of Ag (a), $Pd_{33}Ag_{67}$ (b), $Pd_{50}Ag_{50}$ (c), $Pd_{75}Ag_{25}$ (d), $Pd_{87}Ag_{13}$ (e), Pd (f).

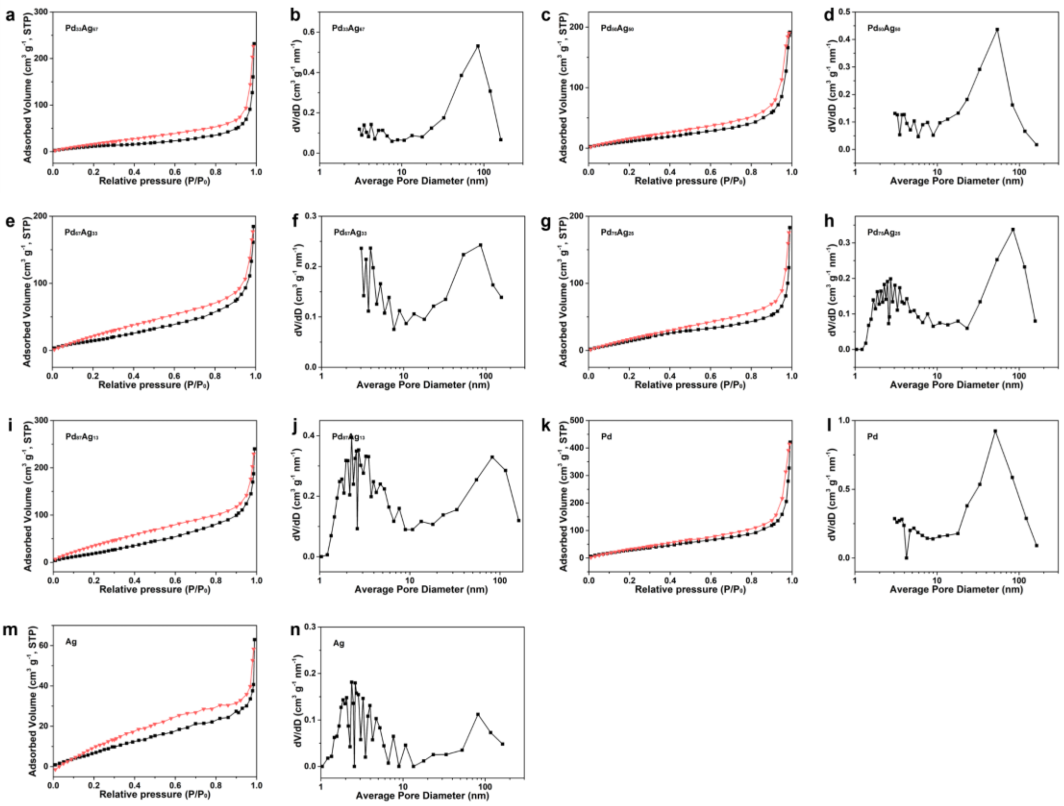

Supplementary Figure 3 N_2 adsorption/desorption isotherms and pore size distribution of $Pd_{33}Ag_{67}$ (a-b), $Pd_{50}Ag_{50}$ (c-d), $Pd_{67}Ag_{33}$ (e-f), $Pd_{75}Ag_{25}$ (g-h), $Pd_{87}Ag_{13}$ (i-j), Pd (k-l), and Ag (m-n).

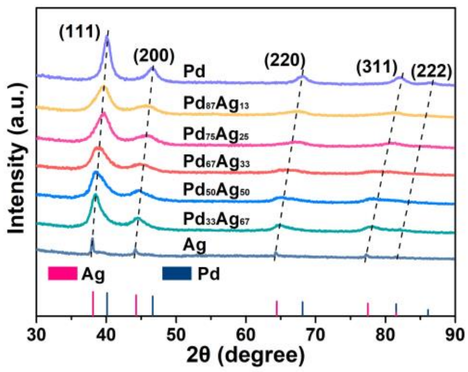

Supplementary Figure 4 XRD patterns of PdAg aerogels with different Pd/Ag ratio.

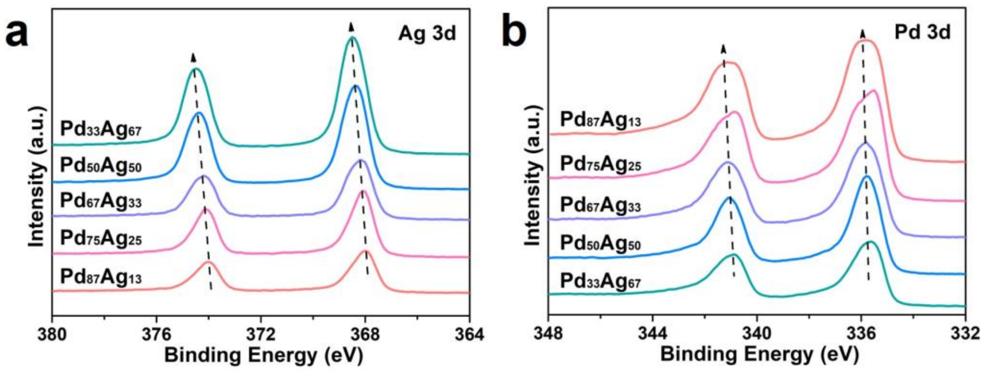

Supplementary Figure 5 Ag 3d (a) and Pd 3d (b) XPS patterns of PdAg aerogels with different Pd/Ag ratio.

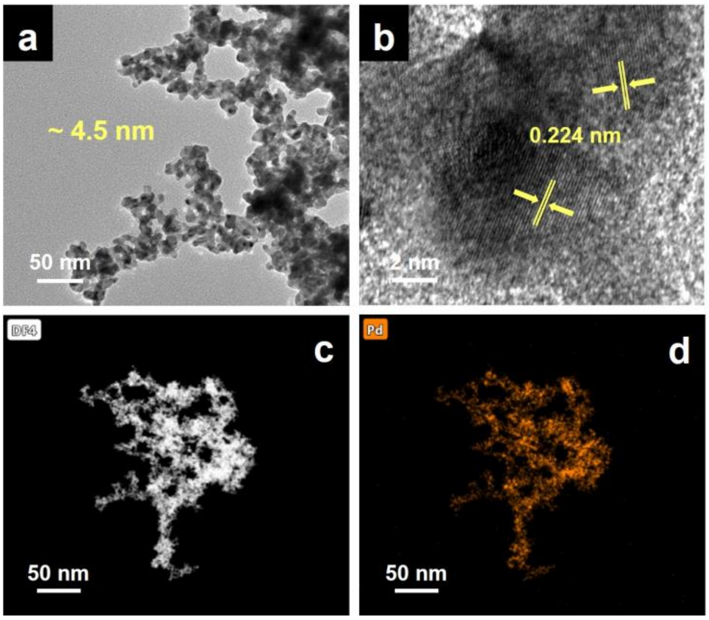

Supplementary Figure 6 HR-TEM images of Pd aerogels.

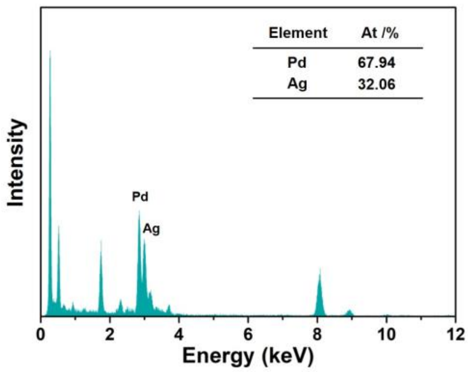

Supplementary Figure 7 TEM-EDS spectrum of $Pd_{67}Ag_{33}$ aerogel.

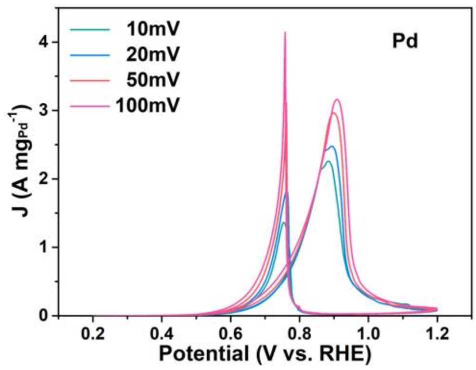

Supplementary Figure 8 CV curves of Pd aerogel in 1 M KOH/1M EG.

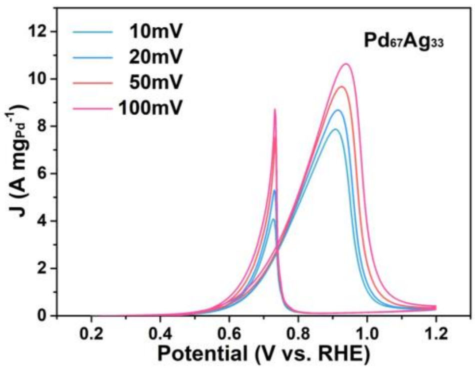

Supplementary Figure 9 CV curves of $Pd_{67}Ag_{33}$ aerogel in 1 M KOH/1M EG.

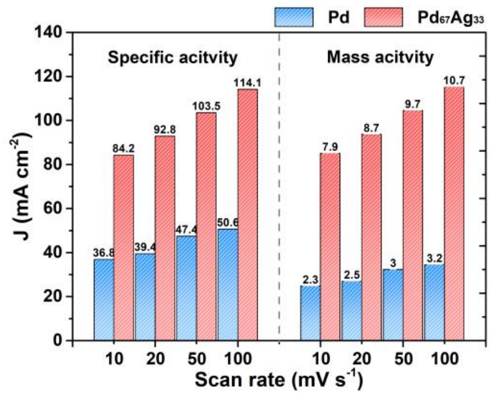

Supplementary Figure 10 Specific and mass activities of the Pd and $Pd_{67}Ag_{33}$ aerogel catalysts for EGOR in 1 M KOH/1 M EG.

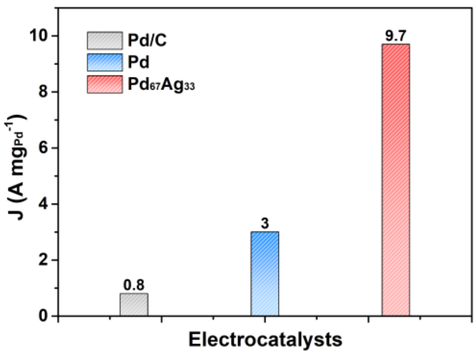

Supplementary Figure 11 Mass activities of EG oxidation over catalysts of Pd/C, Pd aerogel and $Pd_{67}Ag_{33}$ aerogel. Reaction conditions: 1 M EG in 1 M KOH electrolyte at a scan rate of 50 mV s^{-1}.

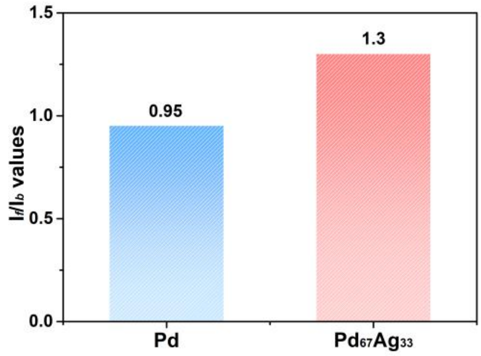

Supplementary Figure 12 Summarized I_f/I_b ratios of Pd and $Pd_{67}Ag_{33}$ aerogel from the CV curves. Reaction conditions: 1 M EG in 1 M KOH electrolyte at a scan rate of 50 mV s^{-1}.

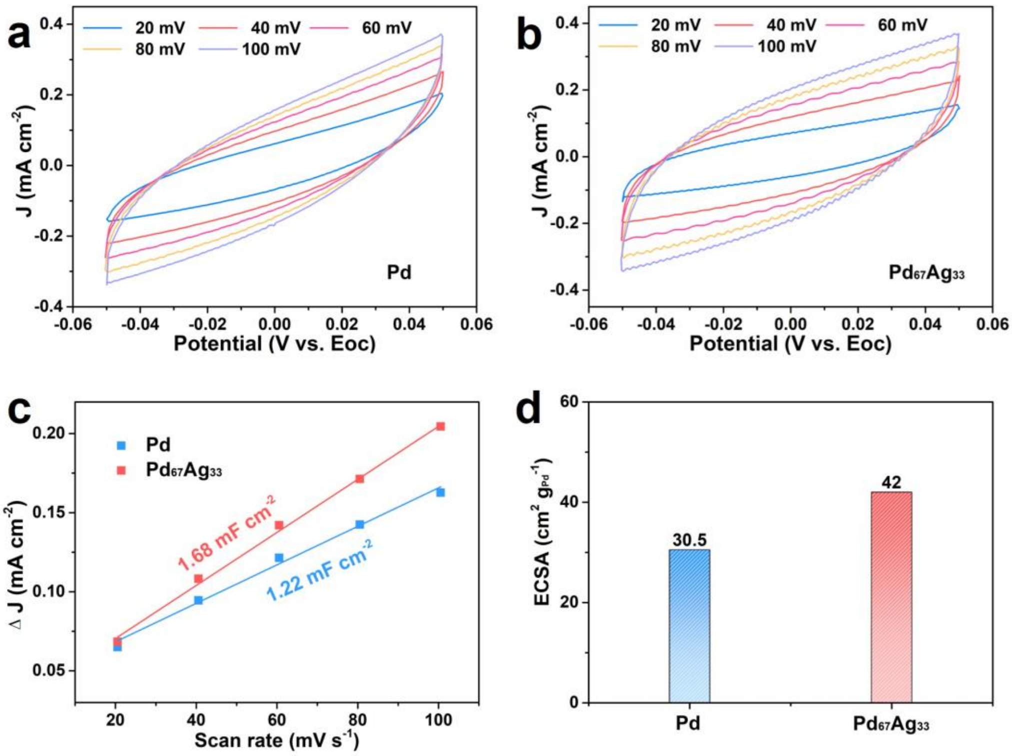

Supplementary Figure 13 CV curves in the non-faradaic regions for Pd (a) and $Pd_{67}Ag_{33}$ (b) aerogel in 1 M KOH/1M EG. (c) The linear relation of ΔJ and scan rates for ECSA tests. (d) Summarized electrocatalytically surface areas.

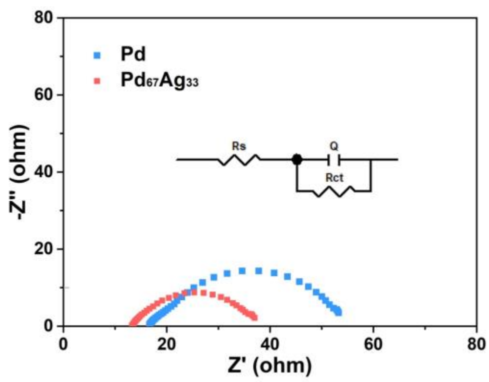

Supplementary Figure 14 EIS Nyquist plots for Pd and $Pd_{67}Ag_{33}$ in 1 M KOH/1M EG (inset is the equivalent circuit models).

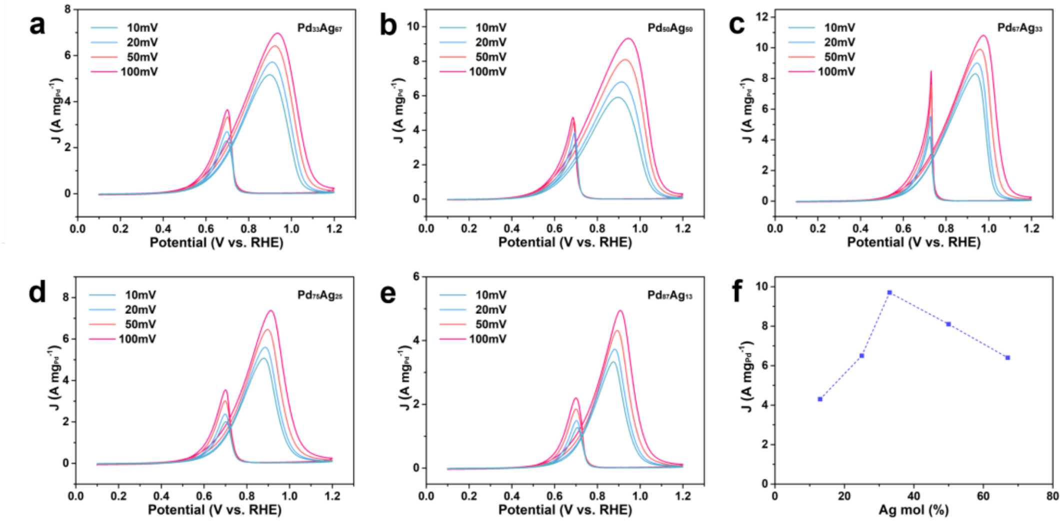

Supplementary Figure 15 Mass activities of EG oxidation over catalysts of $Pd_{33}Ag_{67}$ (a), $Pd_{50}Ag_{50}$ (b), $Pd_{67}Ag_{33}$ (c), $Pd_{75}Ag_{25}$ (d), $Pd_{87}Ag_{13}$ (e), and the comparison of catalysts' mass activities in the EGOR (f). Reaction conditions: 1 M EG in 1 M KOH electrolyte at a scan rate of 50 mV s^{-1}.

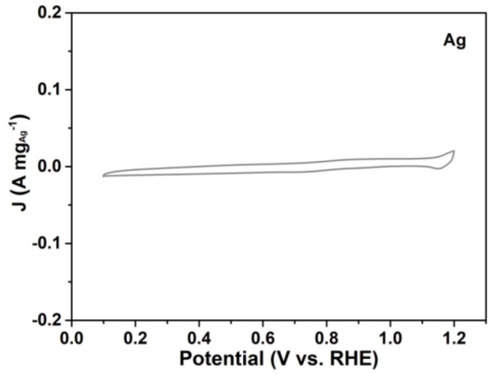

Supplementary Figure 16 Mass activities of EG oxidation over Ag aerogel catalyst.

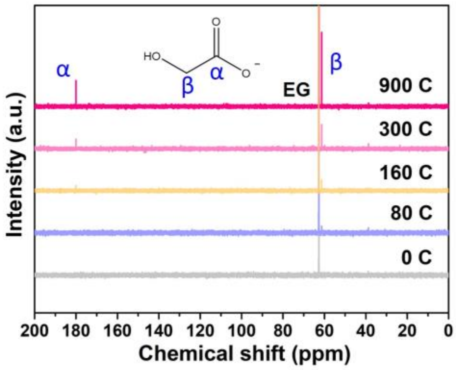

Supplementary Figure 17 ^{13}C NMR spectra of products after electrooxidation on $Pd_{67}Ag_{33}$ electrode with different charges passed.

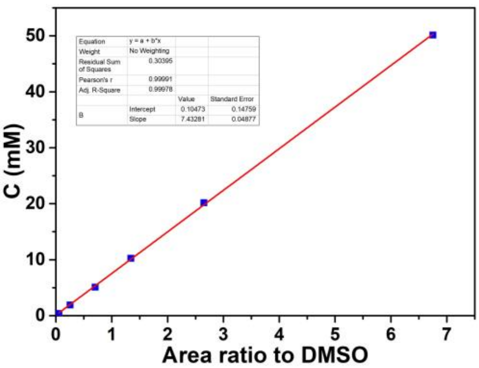

Supplementary Figure 18 The corresponding calibration curve used to quantify the concentrations of the produced GA in the electrolyte.

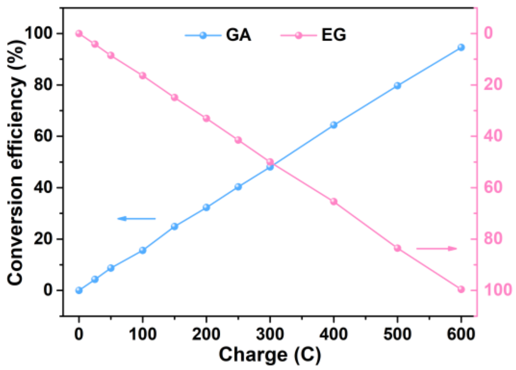

Supplementary Figure 19 The concentration variation of EG and GA during electrolysis within 600 C charge.

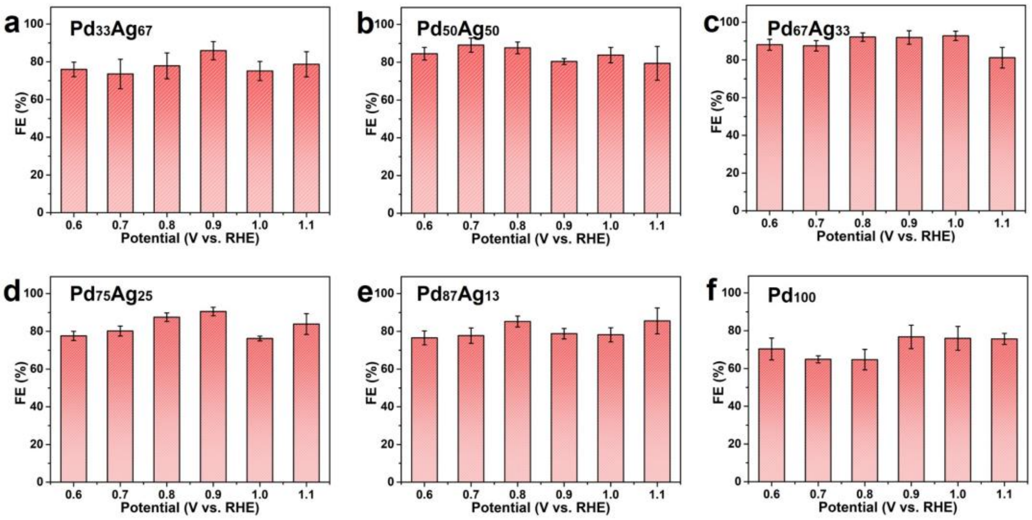

Supplementary Figure 20 Comparison of GA selectivity of PdAg aerogel catalysts with different Pd/Ag ratios.

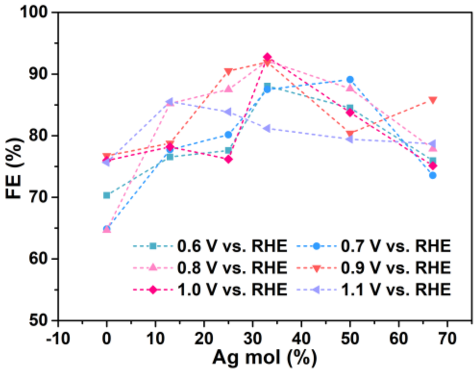

Supplementary Figure 21 Comparison of GA selectivity of PdAg aerogel catalysts at 0.6-1.1 V.

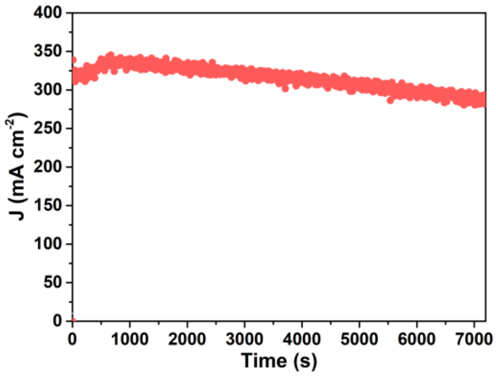

Supplementary Figure 22 Chronoamperometric curve of $Pd_{67}Ag_{33}$ in in 1 M EG/1 M KOH at 1.0 V vs. RHE.

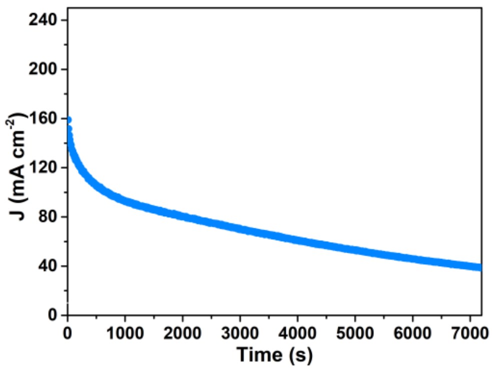

Supplementary Figure 23 Chronoamperometric curve of Pd in 1 M EG/1 M KOH at 1.0 V vs. RHE.

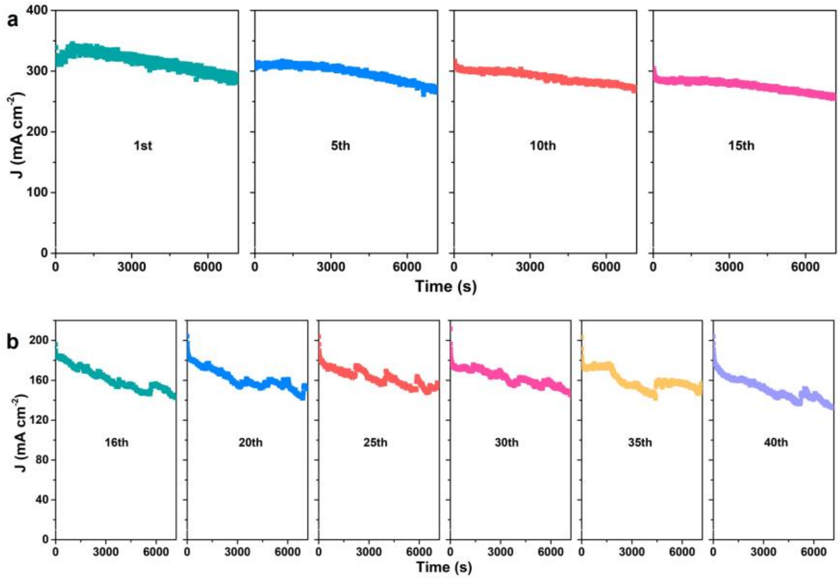

Supplementary Figure 24 Representative chronoamperometric curves of $Pd_{67}Ag_{33}$ during the long-term stability test in 1 M EG/1 M KOH at 1.0 V vs. RHE (a) and 0.9 V vs. RHE (b).

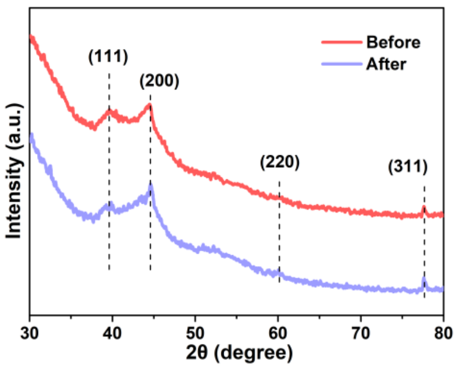

Supplementary Figure 25 XRD patterns of $Pd_{67}Ag_{33}$/CP electrode before and after electrolysis.

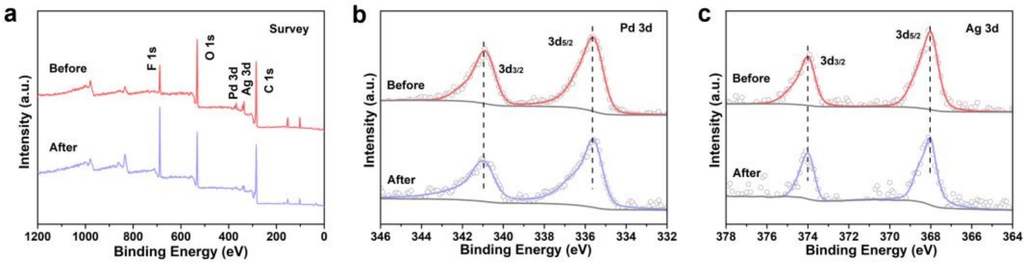

Supplementary Figure 26 XPS spectrums of $Pd_{67}Ag_{33}$/CP electrode before and after electrolysis.

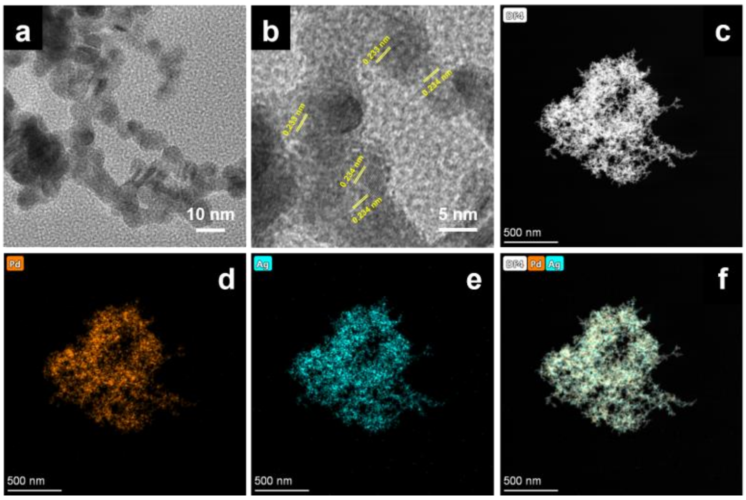

Supplementary Figure 27 TEM image (a-b), HAADF-STEM (c), and corresponding elemental mapping images (d-f) of $Pd_{67}Ag_{33}$ catalyst after electrolysis.

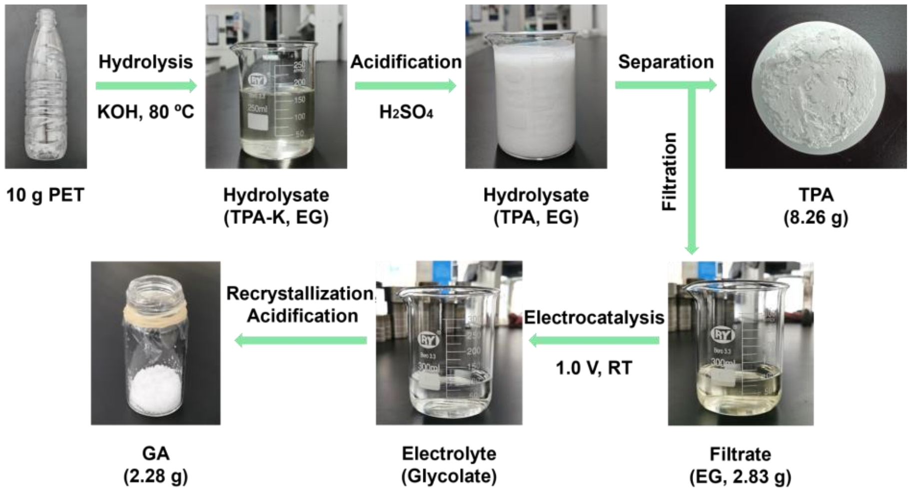

Supplementary Figure 28 Photographs of the electrocatalytic GA synthesis derived from waste PET plastics.

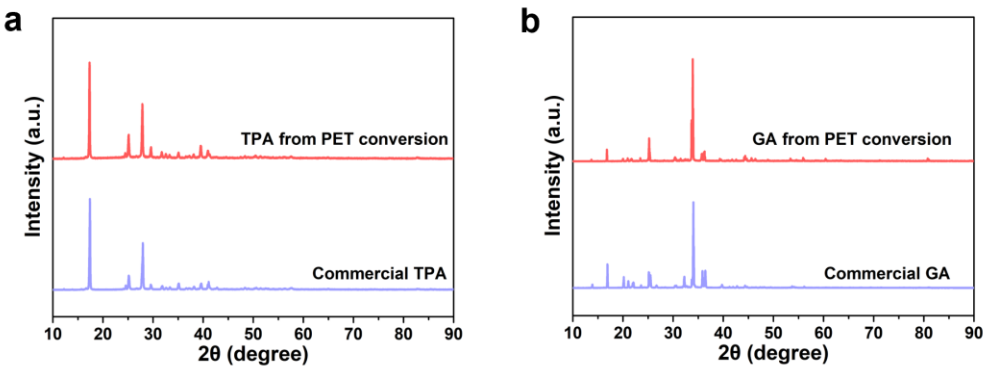

Supplementary Figure 29 XRD for regenerated PTA (a) and GA (b).

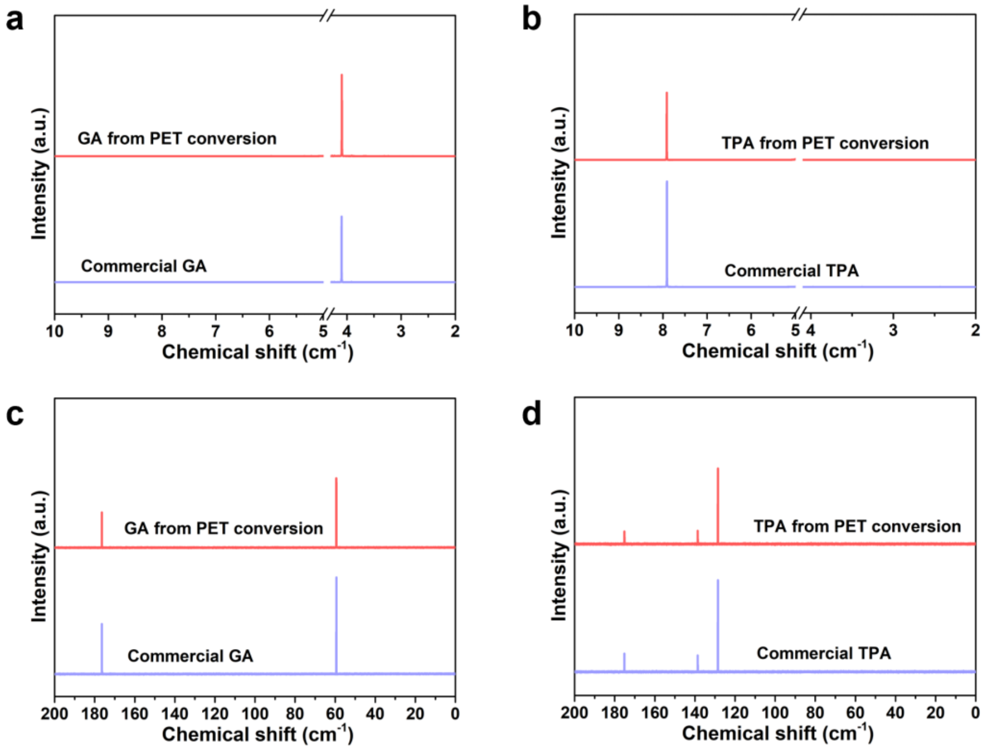

Supplementary Figure 30 ^{1}H NMR and ^{13}C NMR for regenerated TPA and GA.

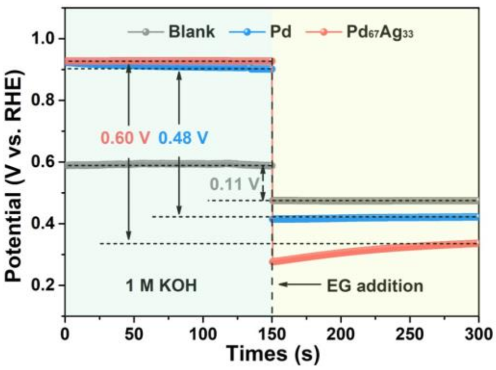

Supplementary Figure 31 OCP of blank glass carbon, Pd, $Pd_{67}Ag_{33}$ in 1 M KOH solution before and after EG addition.

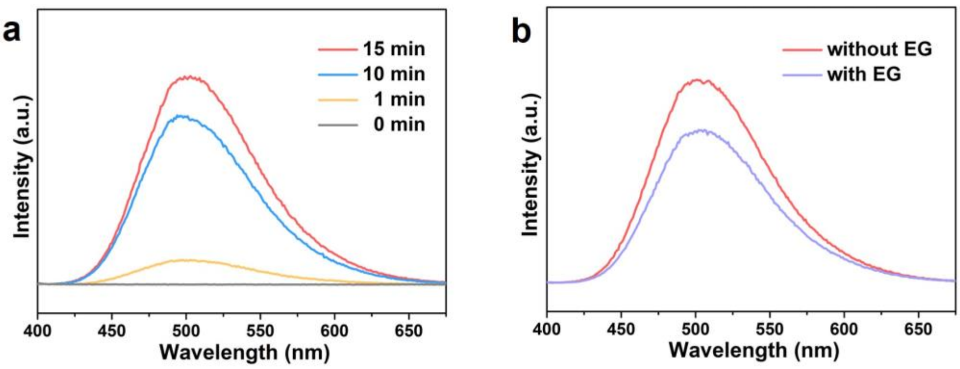

Supplementary Figure 32 (a) Time-dependent fluorescence spectra for the detected •OH radicals in 1 M KOH using a coumarin (0.2 mM) indicator with the excitation wavelength of 350 nm. (b) Fluorescence spectra in 1 M KOH with and without EG.

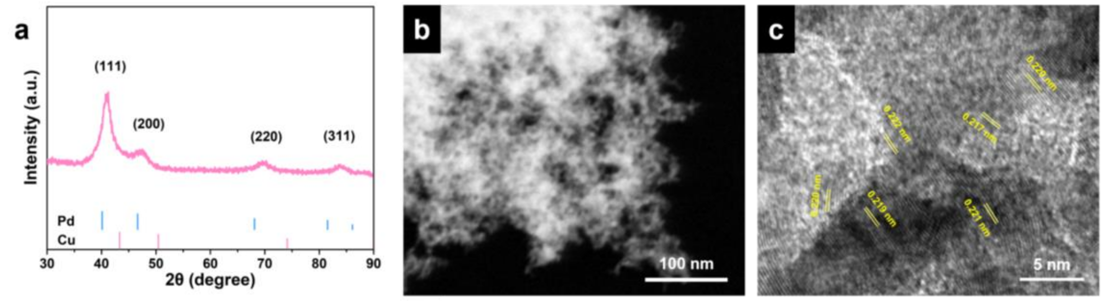

Supplementary Figure 33 (a) XRD pattern, (b) HDDAF-STEM image, and (c) HR-TEM image of $Pd_{67}Cu_{33}$.

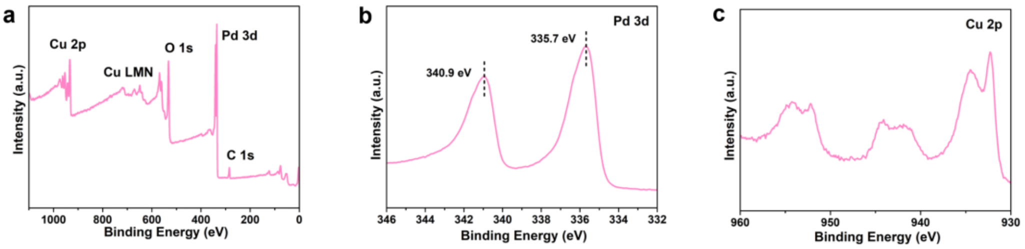

Supplementary Figure 34 (a) XPS spectrum and high resolution XPS spectra of (b) Pd 3d and (c) Cu 2p in $Pd_{67}Cu_{33}$ aerogels

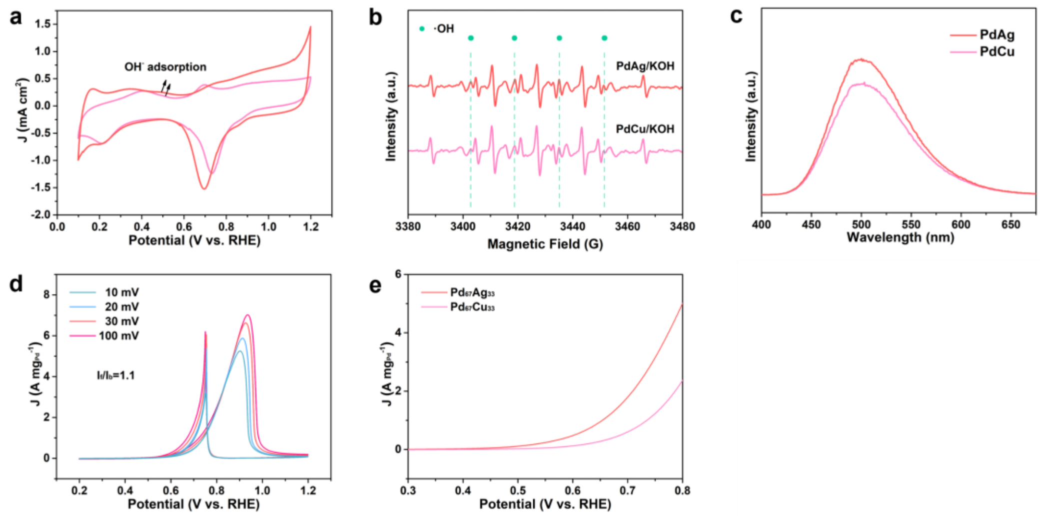

Supplementary Figure 35 (a) Comparation of CV curves upon $Pd_{67}Ag_{33}$ and $Pd_{67}Cu_{33}$ with the electrolyte of 1 M KOH. (b) EPR spectra from the electrolyte from PdAg/KOH and PdCu/KOH systems. (c) Fluorescence spectra for the detected •OH radicals in electrolytes. (d) Mass activities of EG oxidation over $Pd_{67}Cu_{33}$. (e) The local magnified CV curves from Figure d.

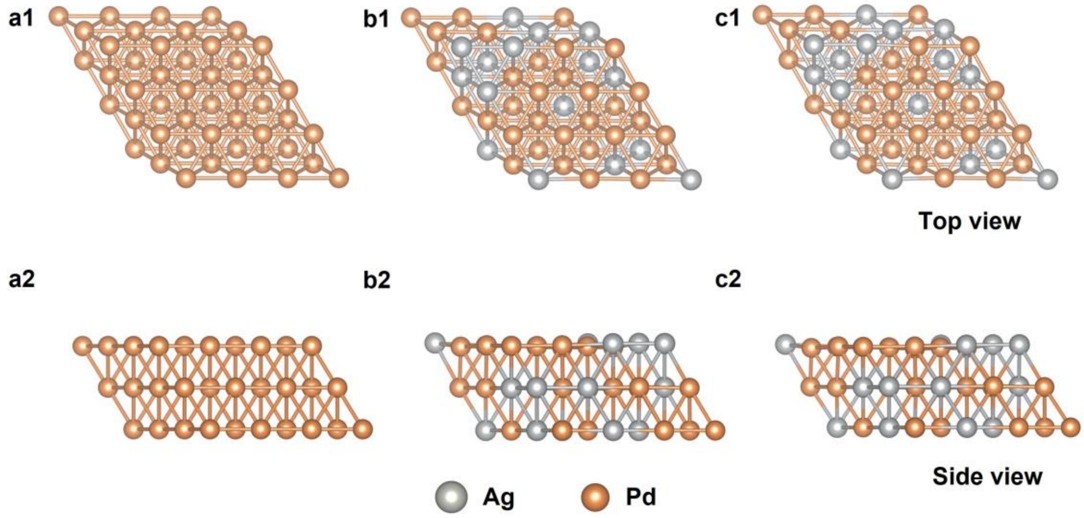

Supplementary Figure 36 Optimized models of Pd (a), $Pd_{67}Ag_{33}$-0% (b) and $Pd_{67}Ag_{33}$ (c).

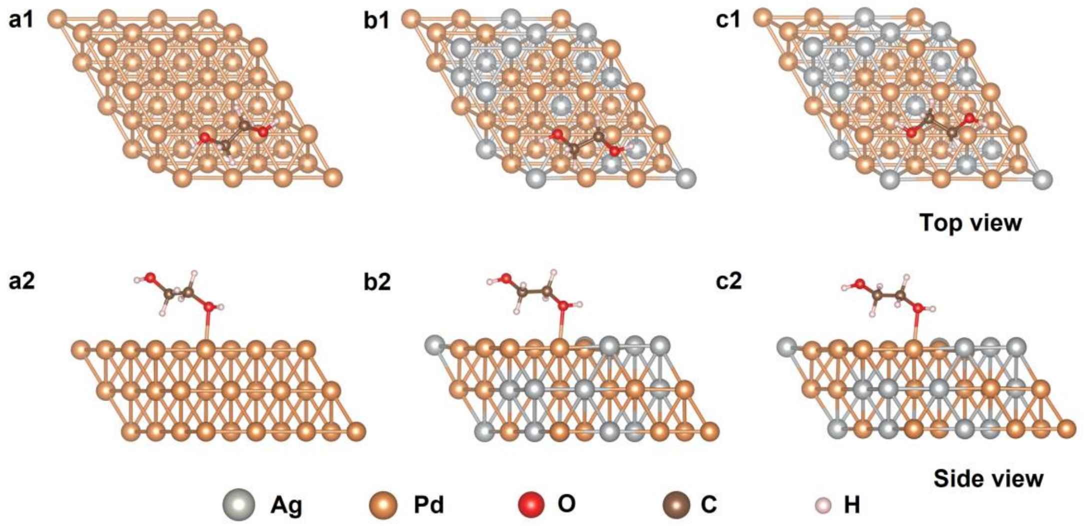

Supplementary Figure 37 Optimized *EG on the (111) plane of Pd (a), $Pd_{67}Ag_{33}$-0% (b) and $Pd_{67}Ag_{33}$ (c).

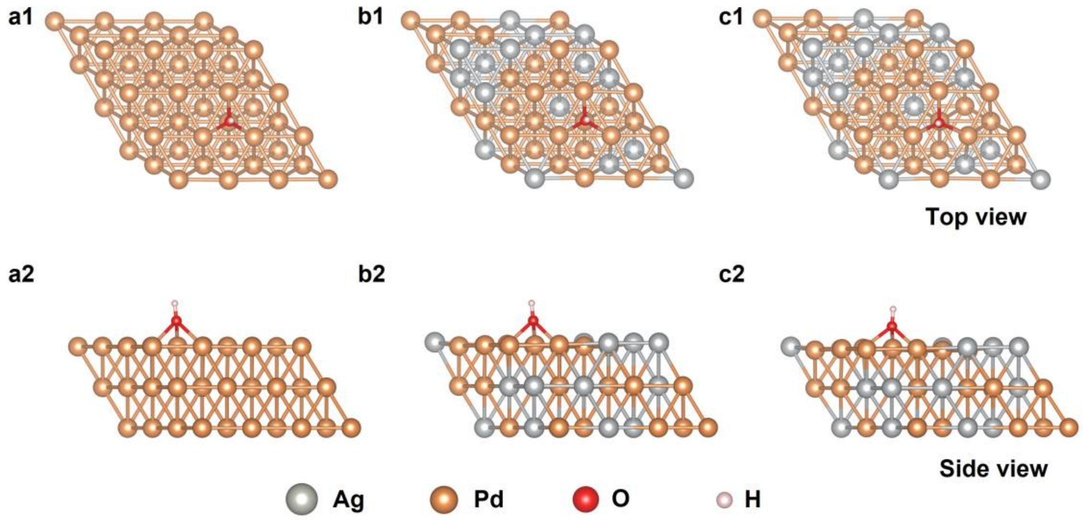

Supplementary Figure 38 Optimized *OH on the (111) plane of Pd (a), $Pd_{67}Ag_{33}$-0% (b) and $Pd_{67}Ag_{33}$ (c).

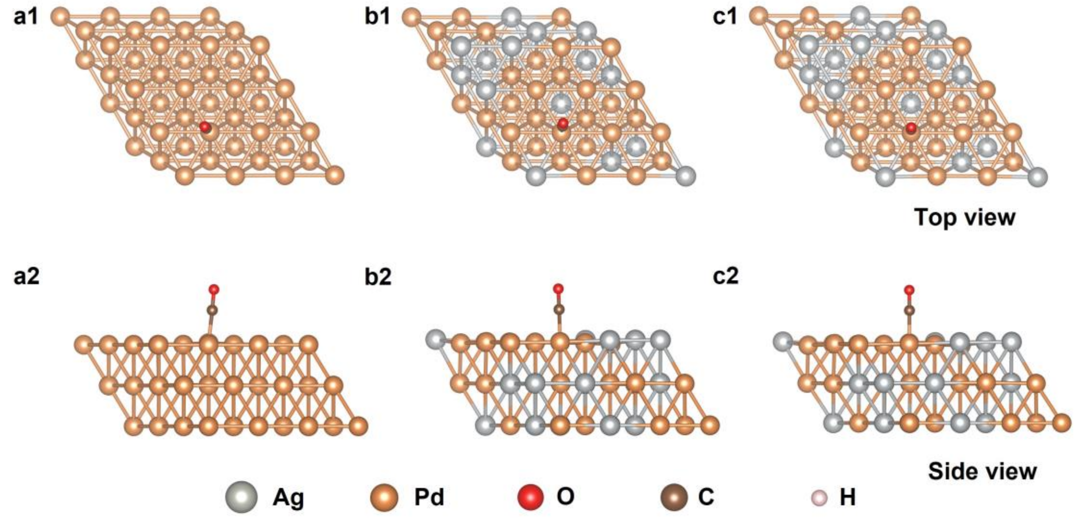

Supplementary Figure 39 Optimized *CO on the (111) plane of Pd (a), $Pd_{67}Ag_{33}$-0% (b) and $Pd_{67}Ag_{33}$ (c).

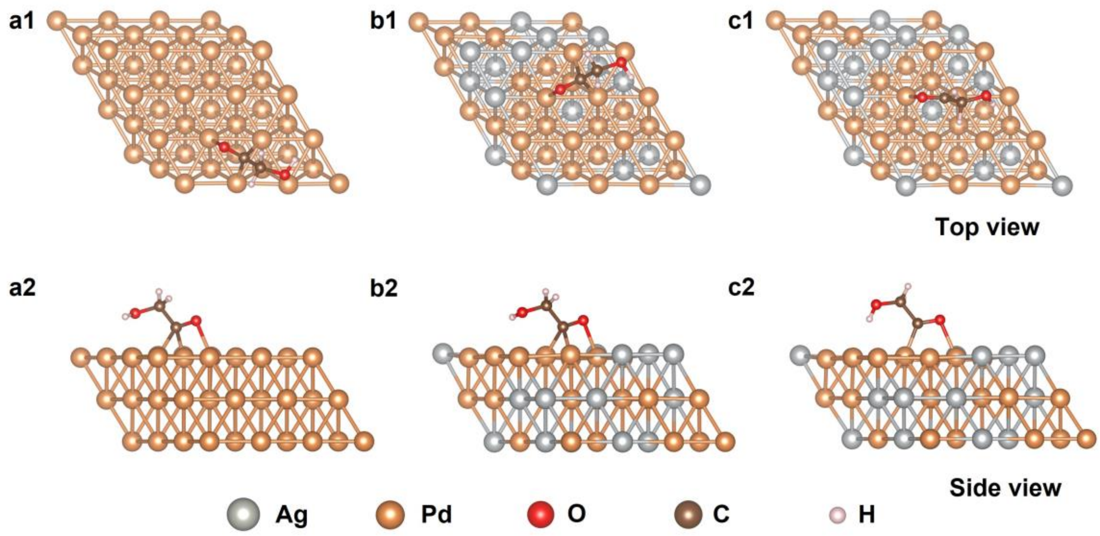

Supplementary Figure 40 Optimized $*OCCH_2OH$ on the (111) plane of Pd (a), $Pd_{67}Ag_{33}$-0% (b) and $Pd_{67}Ag_{33}$ (c).

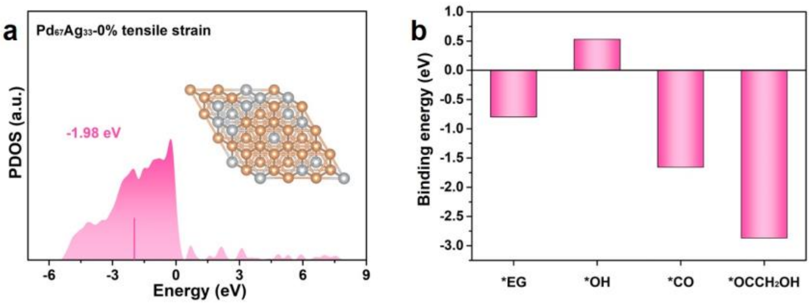

Supplementary Figure 41 (a) PDOS (d-band center) of $Pd_{67}Ag_{33}$-0%. (b) Calculated adsorption energy of *EG, *OH, *CO, *$OCCH_2OH$ on $Pd_{67}Ag_{33}$-0%.

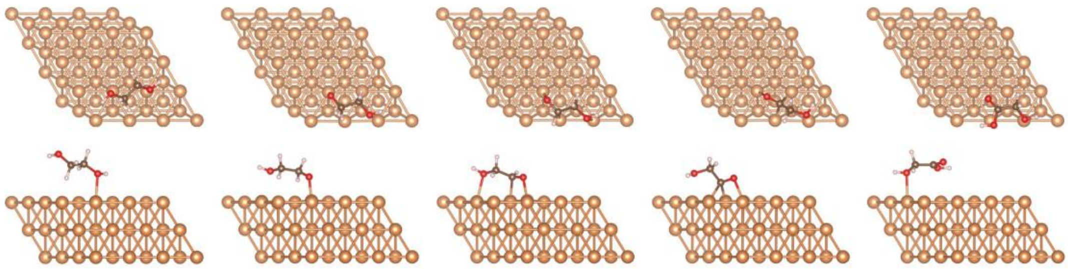

*HOCH2-CH2OH *OCH2-CH2OH *OCH-CH2OH *OC-CH2OH *COOH-CH2OH

Supplementary Figure 42 Optimized surface adduct configurations of the EG oxidation reaction on Pd.

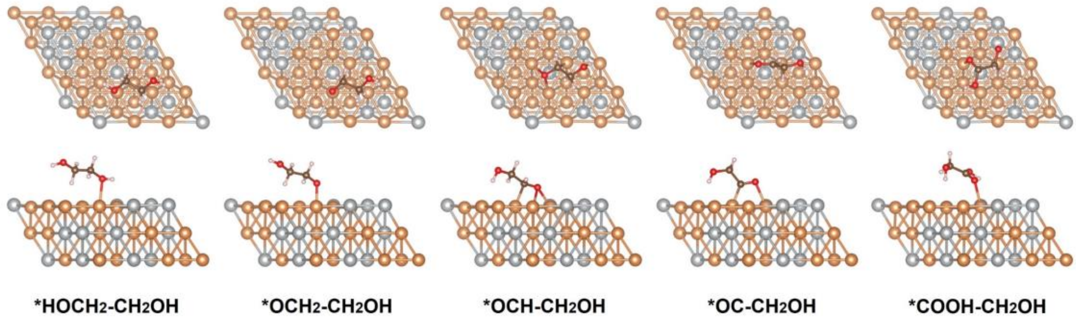

Supplementary Figure 43 Optimized surface adduct configurations of the EG oxidation reaction on $Pd_{67}Ag_{33}$ (with 3.7% tensile strain).

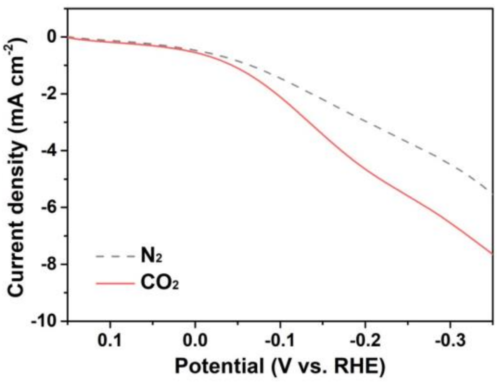

Supplementary Figure 44 CO_2RR polarization curves under N_2 or CO_2 in 0.1 M $KHCO_3$.

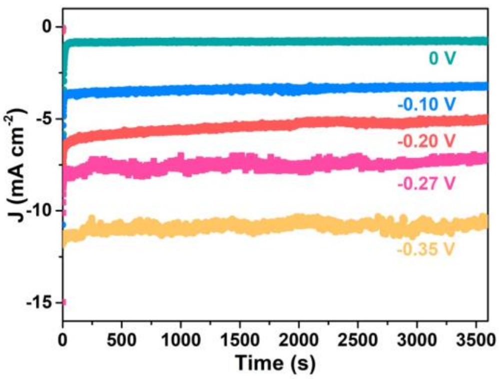

Supplementary Figure 45 Chronoamperometric curves of $Pd_{67}Ag_{33}$ at different potentials.

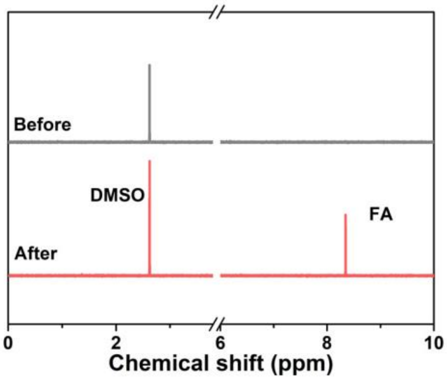

Supplementary Figure 46 ^{1}H NMR spectra of electrolyte before and after CO_2RR test.

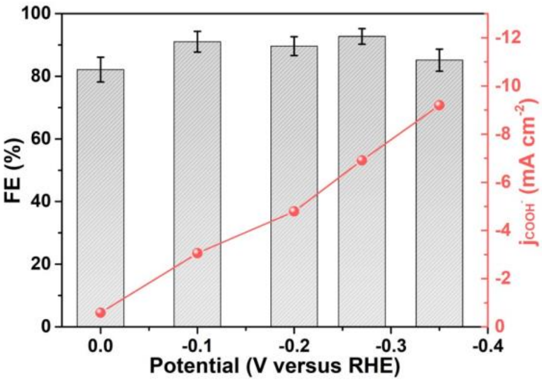

Supplementary Figure 47 Potential-dependent FA Faradaic efficiency and partial current density.

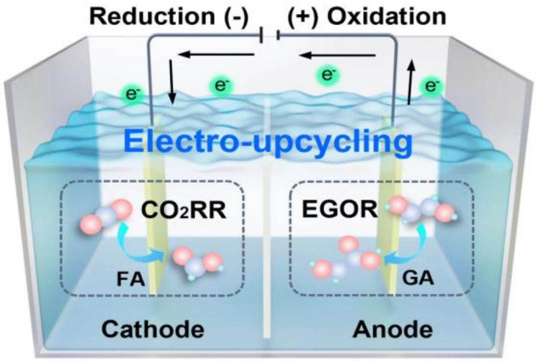

Supplementary Figure 48 Schematic illustration of integrated electrolysis cell coupling EGOR with CO_2RR.

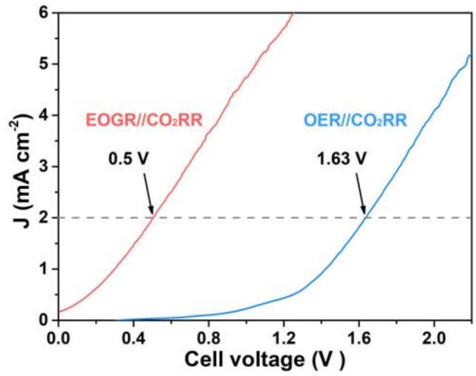

Supplementary Figure 49 LSV curves of the integrated cell in the electrolytes with and without EG.

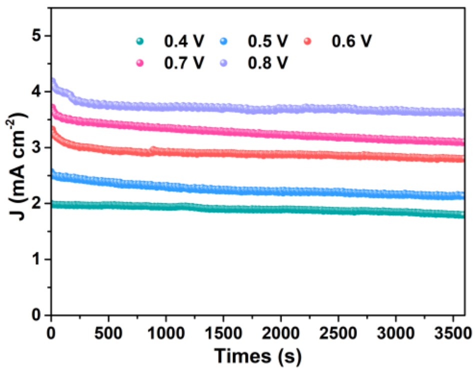

Supplementary Figure 50 Chronoamperometric curves of the EGOR//CO_2RR integrated electrolyzer.

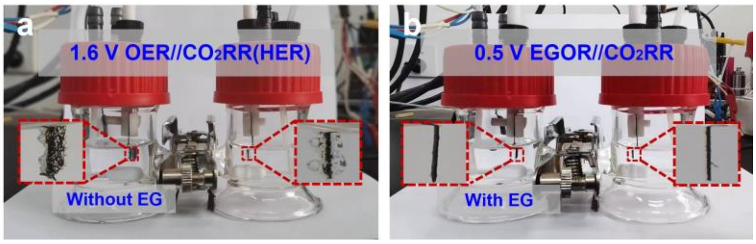

Supplementary Figure 51 Photograph of the two-electrode cell for co-upcycling of PET and CO_2 by using two $Pd_{67}Ag_{33}$ electrodes as anode and cathode with and without EG.

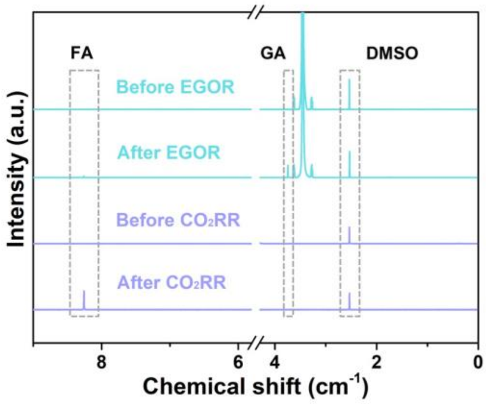

Supplementary Figure 52 The NMR signals for cathodic and anodic products.

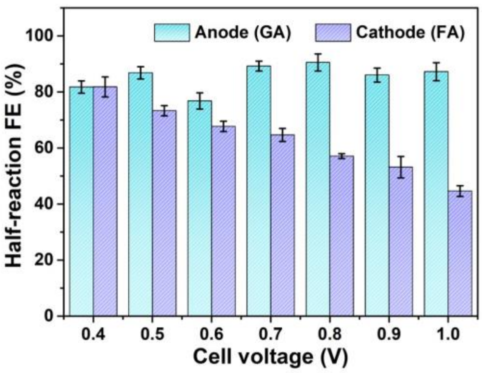

Supplementary Figure 53 FE of GA and FA in the integrated cell.

Table S1 Nitrogen adsorption/desorption data of as-prepared PdAg alloy aerogels.

Samples	S_{BET} **(m^2 g^{-1})**	V_{total} **(cm^3 g^{-1})**
Ag	26.9	0.098
$Pd_{33}Ag_{67}$	52.8	0.359
$Pd_{50}Ag_{50}$	63.5	0.296
$Pd_{67}Ag_{33}$	89.8	0.285
$Pd_{75}Ag_{25}$	98.0	0.284
$Pd_{87}Ag_{13}$	126.2	0.372
Pd	144.8	0.652

Table S2 XPS element analysis data of PdAg alloy aerogels.

	Pd (at%)	**Ag (at%)**
Ag	\	100
$Pd_{33}Ag_{67}$	37.6	63.4
$Pd_{50}Ag_{50}$	46.8	53.2
$Pd_{67}Ag_{33}$	65.2	34.8
$Pd_{75}Ag_{25}$	76.3	23.7
$Pd_{87}Ag_{13}$	88.7	11.3
Pd	100	\

Table S3 Pd-Ag ratio of samples measured by inductively coupled plasma optical emission spectroscopy (ICP-OES).

	Pd (wt%)	**Ag (wt%)**	**Pd (at%)**	**Ag (at%)**
$Pd_{33}Ag_{67}$	40.2	59.8	40.6	59.4
$Pd_{50}Ag_{50}$	49.8	50.2	50.1	49.9
$Pd_{67}Ag_{33}$	68.0	32.0	68.3	31.7
$Pd_{75}Ag_{25}$	77.5	22.5	77.7	22.3
$Pd_{87}Ag_{13}$	88.1	11.9	88.2	11.8

Table S4. The equivalent circuit parameters from EIS analysis.

Samples	R_0 (Ω)	R_{ct} (Ω)
Pd	16.77	40.73
$Pd_{67}Ag_{33}$	15.23	25.72

Table S5 Comparison of the alcohol oxidation performances over noble metal-based catalysts reported in the literatures and in this work.

Catalysts	Electrolyte	Mass activity ($A\ mg_{NM}^{-1}$)	Chronoamperometric stability (%)	Ref.
$Pd_{67}Ag_{33}$ alloys aerogel	**1 M KOH + 1 M EG**	**9.7**	83.8 (7200s)	**This work**
Rh/RhOOH metallene	1 M KOH + 1 M EG	0.63	65.3(10000s)	(1)
SA In-Pt NWs/C	1 M KOH + 0.5 M EG	1.1	70 (2000 cycles)	(2)
Bi/Pd CNCs	1 M NaOH + 1 M EG	1.2	/	(3)
22% YOx/MoOx–Pt	1 M KOH + 1 M methanol	2.1	64.7 (1200 cycles)	(4)
Au@PdPt	1 M KOH + 1 M EG	3	36 (1000 cycles)	(5)
Pd−$WO_{2.75}$ NB	1 M KOH + 1 M EG	4.3	84.8 (1000 cycles)	(6)
Pd_8Sb_3 HPs/C	1.0 M NaOH+1.0 M EtOH	5.2	76.7 (5000s)	(7)
Pd_7Ag NSs	0.5 M KOH + 1 M EG	7.0	37 (3600s)	(8)
Pd-PdSe HNSs	1 M KOH + 1 M EG	8.6	40.5 (5000s)	(9)

Table S6 Comparison of the selective EG-to-GA conversion performances over noble metal-based catalysts reported in the literatures and in this work.

Catalysts	**Electrolyte**	**Mass activity ($A\ mg_{Pd}^{-1}$)**	**Loading mass ($mg\ cm^{-2}$)**	**Potential (V vs. RHE)**	**Current density ($mA\ cm^{-2}$)**	**Faraday efficiency (%)**	**Productivity ($mmol\ cm^{-2}\ h^{-1}$)**	**Ref.**
$Pd_{67}Ag_{33}$ alloys aerogel	**1 M KOH + 1 M EG**	**9.7**	**0.33 mg_{Pd}**	**1.0**	**339**	**92.7**	**2.56**	**This work**
Pd-$Ni(OH)_2$/NF	1 M KOH + 1 M EG	0.78	1.5	1.2	100 (50 °C)	94.1	0.87	(10)
Au/$Ni(OH)_2$	3 M KOH + 0.3 M EG	1.79	0.34 mg_{Au}	1.15	250	91	2.23	(11)
Pd NTs/NF	PET hydrolysate (1 M KOH)	/	/	0.57	10	87.9	/	(12)
Pt/γ-NiOOH/NF	1 M KOH + 1 M EG	2.5	0.18	0.55	90	90.2	0.14	(13)
PdAg/NF	1 M KOH + 1 M EG	/	/	0.91	125	92	0.15	(14)
Pd-N_4/Cu-N_4	1 M NaOH+ 1 M EG	1.9	0.042 mg_{Pd}	1.0	140	91.9	/	(15)

Table S7 Pd-Cu ratio of samples measured by inductively coupled plasma optical emission spectroscopy (ICP-OES).

	Pd (wt%)	**Cu (wt%)**	**Pd (at%)**	**Cu (at%)**
$Pd_{67}Cu_{33}$	76.9	23.1	66.5	33.5

References

1. Q. Mao *et al.*, In Situ Reconstruction of Partially Hydroxylated Porous Rh Metallene for Ethylene Glycol-Assisted Seawater Splitting. *Adv. Funct. Mater.* **32**, 2201081 (2022).
2. Y. Zhu *et al.*, Single-Atom In-Doped Subnanometer Pt Nanowires for Simultaneous Hydrogen Generation and Biomass Upgrading. *Adv. Funct. Mater.* **30**, 2004310 (2020).
3. H. Wang *et al.*, Electrocatalysis of Ethylene Glycol Oxidation on Bare and Bi-Modified Pd Concave Nanocubes in Alkaline Solution: An Interfacial Infrared Spectroscopic Investigation. *ACS Catal.* **7**, 2033-2041 (2017).
4. M. Li *et al.*, Sub-Monolayer YO(x) /MoO(x) on Ultrathin Pt Nanowires Boosts Alcohol Oxidation Electrocatalysis. *Adv. Mater.* **33**, e2103762 (2021).
5. X. Yang *et al.*, Modulating Electronic Structure of an Au-Nanorod-Core–PdPt-Alloy-Shell Catalyst for Efficient Alcohol Electro-Oxidation. *Adv. Energy Mater.* **11**, 2100812 (2021).
6. L. Karuppasamy, C. Y. Chen, S. Anandan, J. J. Wu, Low- and High-Index Faceted Pd Nanocrystals Embedded in Various Oxygen-Deficient WO_x Nanostructures for Electrocatalytic Oxidation of Alcohol (EOA) and Carbon Monoxide (CO). *ACS Appl. Mater. Interfaces* **11**, 10028-10041 (2019).
7. Y. Zhang *et al.*, Rhombohedral Pd-Sb Nanoplates with Pd-Terminated Surface: An Efficient Bifunctional Fuel-Cell Catalyst. *Adv. Mater.* **34**, e2202333 (2022).
8. F. Gao, Y. Zhang, F. Ren, Y. Shiraishi, Y. Du, Universal Surfactant-Free Strategy for Self-Standing 3D Tremella-Like Pd–M (M = Ag, Pb, and Au) Nanosheets for Superior Alcohols Electrocatalysis. *Adv. Funct. Mater.* **30**, 2000255 (2020).
9. Y. Qin *et al.*, Extraordinary p-d Hybridization Interaction in Heterostructural Pd-PdSe Nanosheets Boosts C–C Bond Cleavage of Ethylene Glycol Electrooxidation. *Angew. Chem. Int. Ed.* **61**, e202200899 (2022).
10. F. Liu *et al.*, Concerted and Selective Electrooxidation of Polyethylene-Terephthalate-Derived Alcohol to Glycolic Acid at an Industry-Level Current Density over a Pd-$Ni(OH)_2$ Catalyst. *Angew. Chem. Int. Ed. Engl.* **62**, e202300094 (2023).
11. Y. Yan *et al.*, Electrocatalytic Upcycling of Biomass and Plastic Wastes to Biodegradable Polymer Monomers and Hydrogen Fuel at High Current Densities. *J. Am. Chem. Soc.* **145**, 6144-6155 (2023).
12. T. Ren *et al.*, Electrochemical Co-Production of Ammonia and Biodegradable Polymer Monomer Glycolic Acid via the Co-Electrolysis of Nitrate Wastewater and Waste Plastic. *ACS Catal.* **13**, 10394-10404 (2023).
13. M. Du *et al.*, Electrochemical Production of Glycolate Fuelled By Polyethylene Terephthalate Plastics with Improved Techno-Economics. *Small* **19**, 2303693 (2023).
14. D. Si, B. Xiong, L. Chen, J. Shi, Highly selective and efficient electrocatalytic synthesis of glycolic acid in coupling with hydrogen evolution. *Chem Catalysis* **1**, 941-955 (2021).
15. E. A. Moges *et al.*, Sustainable Synthesis of Dual Single-Atom Catalyst of Pd−N_4/Cu−N_4 for Partial Oxidation of Ethylene Glycol. *Adv. Funct. Mater.* **32**, 2206887 (2022).